




CH₃NH₃PbI₃ Perovskite Nanorods Saturable Absorber for Stable Ultra-Fast Laser

Tenghu Cheng , Jianhua Chang , Tengfei Dai, Xiang Liu , Haibin Ni, Liyun Hao, and Jun Sun

Abstract—In this paper, we propose a novel ultrafast laser with nanostructure CH₃NH₃PbI₃ nanorods, yielding a higher modulation depth and lower optical loss. Our experiment is performed through nanopatterned CH₃NH₃PbI₃ rods and an all-solid-state passive mode-locked laser system. The prepared nanoarray CH₃NH₃PbI₃ perovskite exhibits a modulation depth of 8.1% under a saturation intensity of 9.53 MW/cm². By applying the CH₃NH₃PbI₃ nanoarray as a saturable absorber in the ultrafast 1064-nm laser system, a mode-locked pulse with a 30-ps pulse width and an 87.3-MHz repetition rate is achieved. A maximum output power of 542 mW was measured, under an absorption pump power of 5.4 W. With the new structured CH₃NH₃PbI₃, our experiment verifies a new method in ultrafast lasers with low light loss, which potentially uncovers an avenue to develop ultrafast lasers.

Index Terms—CH₃NH₃PbI₃ nanorods, saturable absorber, mode-locked.

I. INTRODUCTION

ULTRAFast lasers are widely used in industrial processing, scientific research and other fields, so methods to achieve ultrafast pulse output attract extensive attention. Theoretically, mode locking is an effective method to achieve ultrashort pulses. Such techniques can be divided into active mode locking and passive mode locking. Compared to active mode locking, passive mode locking can obtain pulses with narrower width and higher quality without adding complex active modulator components in resonator of the lasers, and is also more simple and cheaper to operate. Saturable absorber (SA) is a core element to achieve passive mode locking, where its performance directly affects stability of the mode-locking state and optical parameters of the output pulse [1]–[3]. Different

types of saturable absorbers have been developed and used in lasers, where the most typically researched saturable absorber is the semiconductor saturable absorption mirrors (SESAM), for their suitable saturated absorption characteristics and modulation depth. However, such saturable absorbers face difficulties for complex preparation processes, narrow working band widths and low damage thresholds [4], [5], limiting their widespread application in lasers. Recently, many types of two-dimensional layered materials with excellent optical properties have been gradually discovered. However, such two-dimensional materials also face many problems and have limitations in range of their applications. For example, graphene has a particularly low optical absorption and a small modulation depth [6], [7]. The transition metal sulfide represented by MoS₂, which has a large band gap and a short working band, is mostly applied in the visible-light range [8], [9]. Black phosphorus is difficult to prepare over a large area and easily oxidized in air [10], [11].

Inorganic perovskite has a tunable direct band gap structure and is becoming one of the most promising optoelectronic materials, due to its simple preparation process, low cost and high performance in optoelectronic devices [12]–[14]. By changing different ions and simultaneously change the structure and properties of the material, perovskite materials can adjust the band-gap width which resulted in tunable luminous spectrum (covering the entire visible spectrum) and adjustable optical characteristics [15]–[18]. If Pb²⁺ is replaced by Sn²⁺, the band gap can be as low as 1.2 eV, which can absorb infrared light [14]. In the perovskite materials, CH₃NH₃PbI₃ has considerable solubility in various solvents and can be deposited on any substrate, and films with uniform surface crystallization can be prepared at room temperature [19]–[22]. Through relevant literatures, we understand good saturation absorption characteristics of the CH₃NH₃PbI₃ at 0.5 μm [23], 0.8 μm [24], 1.0 μm [24], 1.5 μm [25] and 2 μm [26]. In 2016, Yan Zhou [22] *et al.* applied CsPbBr₃ nanocrystals as saturable absorbers in ytterbium fiber lasers and achieved an output of 1064-nm mode-locked pulses with a pulse width of 216 ps and a maximum average output power of 10.5 mW. A 1.06-μm passive Q-switched laser based on CH₃NH₃PbI₃-SA was also reported, with pulse width of 305 ns and the maximum average output power of 29 mW [23]. In 2019, Jiang Wang *et al.* [28] reported a low-loss CH₃NH₃PbI₃ thin film as a saturable absorber for a passively Q-switched Nd:YAG laser, which is deposited on a quartz plate. Wideband linear transmittance in the range of 0.3–1.1 μm and nonlinear absorption at 1064 nm were measured. The CH₃NH₃PbI₃-SA has good nonlinear saturation absorption with a modulation

Manuscript received 25 April 2022; revised 4 July 2022; accepted 12 July 2022. Date of publication 18 July 2022; date of current version 26 July 2022. This work was supported in part by the National Natural Science Foundation of China under Grants 61875089 and 62175114 and in part by the Jiangsu Students' Platform for Innovation and Entrepreneurship Training Program under Grant 202010300040. (Corresponding authors: Jianhua Chang; Xiang Liu.)

Tenghu Cheng, Jianhua Chang, Tengfei Dai, and Haibin Ni are with the School of Electronics and Information Technology, Nanjing University of Information Science and Technology, Nanjing 210096, China, and also with the Jiangsu Collaborative Innovation Center of Atmospheric Environment and Equipment Technology, Nanjing University of Information Science & Technology, Nanjing 210044, China (e-mail: 20201218009@nuist.edu.cn; jianhuachang@nuist.edu.cn; 18252583667@163.com; nihaibin@nuist.edu.cn).

Xiang Liu and Liyun Hao are with the School of Electronics and Information Technology, Nanjing University of Information Science and Technology, Nanjing 210096, China (e-mail: xjlx1906@126.com; haoliyun045@163.com).

Jun Sun is with the School of Electrical and Information Engineering of Jiangsu University, Zhenjiang 212013, China (e-mail: sun2000jun@ujs.edu.cn).

Digital Object Identifier 10.1109/JPHOT.2022.3191684

depth of 3.9% and a saturation strength of 6.5 MW/cm². A stable Q-switched laser with a maximum average output power of 388 mW and a pulse width of 192 ns was obtained by using this method. Unlike fiber lasers, bulk all-solid-state lasers have larger resonance losses and more serious beam divergence, so it is very important to reduce the optical losses in these resonators. In recent years, perovskite films have been used as saturable absorbers in all solid-state lasers and fiber lasers, whereas the perovskite with the thin film structure have high reflection of the light, which will result greater loss in the cavity and have difficulty in implement patterning [16]–[19]. The columnar structure is more advantageous in light absorption, which can enhance the light coupling effect and reduce losses. CH₃NH₃PbI₃ nanoarrays have not been reported to be use in all solid-state lasers as SAs. Therefore, it is particularly important to study how to improve the absorption of perovskite and realize its structure.

In this paper, we prepare a vertical perovskite nanoarray to reduce the optical loss and enhance the light absorption of CH₃NH₃PbI₃ to improve the optical properties of device, including depth of the modulation and intensity of the saturation. The vertical perovskite nanoarray is prepared using Radio frequency (Rf) magnetron sputtering technology on anodic alumina (AAO) thin film. Saturation-absorption characteristics of the CH₃NH₃PbI₃ are simulated and verified by experiments, and nonlinear absorption characteristics of the CH₃NH₃PbI₃ are also measured. With the CH₃NH₃PbI₃ as a SA in the passive mode locked Nd:YVO₄ all-solid-state laser, stable mode-locked pulses with a width of 30 ps and a repetition rate of 87.3 MHz are achieved. Center wavelength of the mode locked laser is at 1064.61 nm. A maximum output power of 542 mW is achieved under an absorbed pump power of 5.4 W. Using the newly structured CH₃NH₃PbI₃ perovskite as the absorber, we can produce ultrafast lasers with a more stable and low-cost method.

II. PREPARATION AND CHARACTERIZATION OF THE CH₃NH₃PbI₃-SA

The device is fabricated on a quartz substrate using a combined method of RF-magnetron sputtering technology and anodic alumina (AAO) thin film. First, the substrate is ultrasonically cleaned in acetone, ethanol and deionized water, and then it is treated in an ultraviolet ozone machine to completely remove the organic pollutants adhered to the surface of the substrate. Next, the anodic alumina (AAO) thin film is transferred to the substrate surface. Ultrathin AAO film has a layer of polymethyl methacrylate (PMMA) as the supporting layer, so the most important thing in this transfer is to dissolve PMMA with acetone solution. The PMMA on surface of the AAO film is dissolved with acetone solution in a fume hood. Then, the lead metal (Pb) is sputtered into the AAO hole by RF-magnetron sputtering technology. In the entire sputtering process, metallic lead is used as the sputtering target, argon is used as the sputtering gas. The sputtering pressure, sputtering power and sputtering time are maintained at approximately 1.5 Pa, 30 W and 15 s, respectively. Then, lead oxide (PbO) is generated by oxidizing the substrate in an ultraviolet ozone machine. And deposition is done by putting the precursor solution (50 mg CH₃NH₃I powder

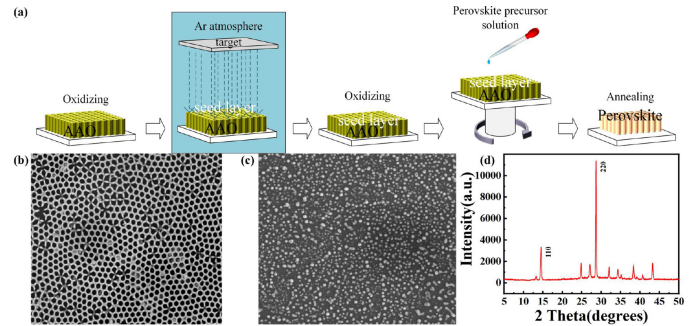


Fig. 1. Preparation and characterization of perovskite nanoarrays. (a) Schematic diagram of the CH₃NH₃PbI₃ prepared by sputtering Metal Pb; (b) TOP view SEM of AAO; (c) Top view SEM of perovskite nanoarrays; (d) XRD patterns of the perovskite thin film.

mixed with 2 mL dimethyl sulfoxide solution) using a pipette on the AAO surface, waiting a minute, and spin-coating with a speed of 3000 rpm for a minute, an extra precursor is added on the template surface to grow longer. Finally, the template was put on a hot plate at 70 °C for 30 min. Preparation process of the CH₃NH₃PbI₃ nanoarrays prepared by sputtering Pb is shown in Fig. 1(a), and details of this process are described as above.

To obtain the microstructure of the prepared CH₃NH₃PbI₃-SA, its surface morphology was characterized by scanning electron microscopy (SEM), as shown in Fig. 1. The Regular pores observed in Fig. 1(b) indicates that the ultrathin AAO film was successful transferred. Top-view SEM of the perovskite nanorods is illustrated in Fig. 1(c), and the small columnar structure of the bulge can be clearly observed, which also indicates that the perovskite nanoarrays grew well. In addition to the morphology information, crystal structure of the CH₃NH₃PbI₃ thin film is studied by X-ray diffraction (XRD). As shown in Fig. 1(d), two dominant peaks appeared at $2\theta = 14.56^\circ$ and 28.7° , which correspond to faces (110) and (220), of the organic–inorganic halide perovskite [24]. Other peaks measured are more than two orders smaller in magnitude.

To get better performance of the device, the reflection characteristics of the periodic micro/nanostructure, was simulated and calculated by the finite difference time domain (FDTD) method. The model built is shown in Fig. 2(a). The columns in the model represent the perovskite material, the blank area represents the air, and the quartz glass is designed at the bottom. As shown in Fig. 2(b) and (d), reflectivity of the device decreased from 4.3% to 3.403% in the wavelength range of 800–1200 nm, benefiting from the nano-column structure with more light interacting with the device, which enhance the coupling effect of light. Fig. 2(c) illustrates influence of the nano-rod diameter on reflectivity of the device. When the aperture is in the range of 200–300 nm with equal thickness, size of the aperture has obvious influence on absorption rate of the device. However, the reflectivity of the device does not change significantly in the wavelength range of 800–1200 nm when the diameters are 200 nm, 300 nm and 350 nm, as shown in Fig. 2(d). From our simulation, an AAO film with an aperture of approximately 350 nm and a thickness of approximately 550 nm is finally used to fabricate the entire device.

Optical absorption spectra of the prepared perovskite saturable absorber are also measured by a grating spectrometer,

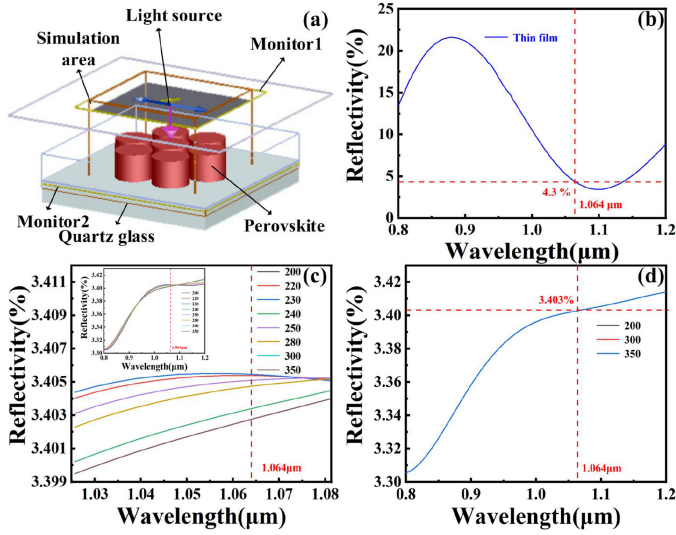


Fig. 2. Simulation results of the refractivity. (a) The simulation model; (b) Reflectivity of the film; (c) Influence of the aperture on the reflectivity of device; (d) Reflectivity of the nanorods.

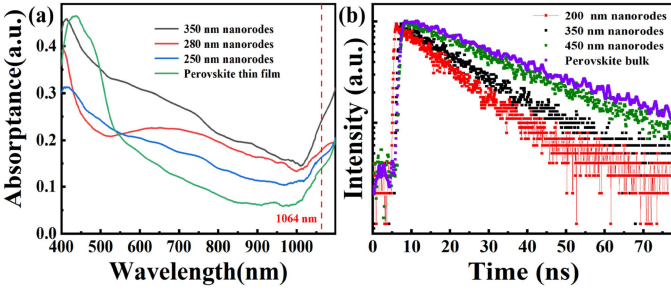


Fig. 3. Optical properties of the devices (a) absorption spectrum; (b) Carrier lifetime comparison between the nanorods and the thin films.

as shown in Fig. 3(a). All the perovskites show strong absorption performance in the wavelength range of 400–1100 nm, mainly coming from the optical transition between the conduction band and the valence band [27]. Compared with the 250 nm and the 280 nm, the 350-nm nanorods had stronger absorption than those at 600–1100 nm, especially at 1064 nm, which is in consistent with our simulation above.

The relationship between carrier lifetime and excess concentration can be expressed as follows:

$$\tau = \frac{\Delta p}{U_d} = \frac{1}{r(n_0 + p_0 + \Delta p)}, \quad (1)$$

where τ is the carrier lifetime, $n_0 + p_0$ is the equilibrium concentrations, U_d is the net composite ratio, r is the compound probability depending only on the temperature, and Δp is the excess concentration. As shown in Fig. 3(b), the columnar perovskites have more contact area with light, which results in a higher concentration of nonequilibrium carriers in the device and reduces its lifetime [30]. The decrease of unbalanced carrier lifetime affects the absorption of light, increases the modulation depth and shortens the pulse width.

Nonlinear transmission characteristic plays an essential role in measuring performance of the saturable absorber. Within a

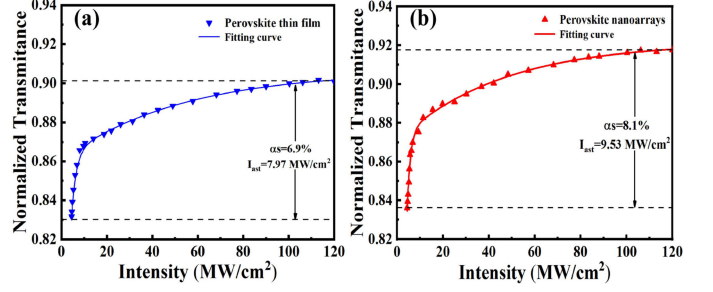


Fig. 4. Modulation depth measurement and the corresponding fitting curve of the different structured devices. (a) Perovskite thin film and (b) Perovskite nanorods.

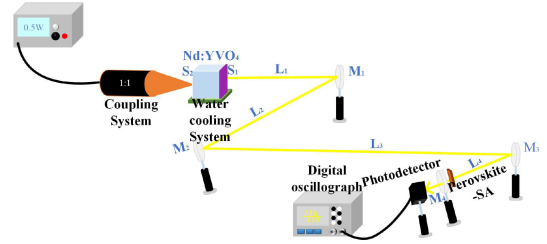


Fig. 5. Schematic diagram of the passive mode-locked laser system.

certain range, a greater modulation depth makes more easily self-start of the mode locking. The nonlinear optical transmission data of two different structures are measured by a balanced synchronous twin-detector measurement system at 1064 nm, as shown in Fig. 4. The laser source is a passively Q-switched pulsed laser with 1064-nm central wavelength, 4-ns pulse width and 10-kHz repetition rate. The experimental data are fitted by the following equation:

$$T(I) = 1 - \alpha_s \exp(-I/I_{sat}) - T_{ns}, \quad (2)$$

where $T(I)$ is the transmission, α_s is the modulation depth, I is the input intensity, I_{sat} is the saturation intensity, and T_{ns} is the non-saturable loss. As shown in Fig. 4(b), saturation intensities of the two different structures are 7.97 MW/cm² and 9.53 MW/cm², corresponding to α_s of 6.9% and 8.1% respectively. The results show that the modulation depth of the columnar structure is higher, deriving from the increase in the carrier concentration of perovskite. With increasing laser intensity, the transmission rate gradually increased and finally reached the saturation state, which indicates that both perovskite thin film and perovskite nanorods have saturable absorption characteristics at 1064 nm.

III. EXPERIMENTAL SETUP

Schematic of the mode-locked laser based on the CH₃NH₃PbI₃-SA is shown in Fig. 5. The pump source is a fiber-coupled LD with a central wavelength of 808 nm. Core diameter and numerical aperture of the fiber pigtail are 400 μ m and 0.22, respectively. The pump beam is focused on the Nd:YVO₄ crystal with a beam radius of 200 μ m using a 1:1 coupling system. The laser gain medium is a finely polished a-cut Nd:YVO₄ crystal with an Nd³⁺ doping concentration of

0.5 at.% and dimensions of $3 \text{ mm} \times 3 \text{ mm} \times 5 \text{ mm}$. To efficiently reduce the thermal effects, the Nd:YVO₄ crystal is wrapped in indium foil and fixed in a copper block, and surface temperature of the crystal is maintained at 25 °C by a water cooling system.

The resonator cavity consists of a laser gain medium, three folding mirrors (M₁, M₂ and M₃), and an output mirror (M₄). The left side (S₁) of the Nd:YVO₄ crystal, which acted as the input mirror, is coated with anti-reflection (AR) at 808 nm and high-reflection (HR) at 1064 nm. The right side (S₂) of the crystal is coated with AR at 1064 nm. The folding mirror M₁, which is coated with HR at 532 nm and 1064 nm on the left side, is a flat mirror. Both folding mirrors M₂ and M₃ are plano-concave mirrors and coated with HR at 532 nm and 1064 nm on the concave sides, and their radii of curvature are 500 mm and 204 mm respectively. The output mirror M₄ is a flat mirror with transmission of 5%. Folding angles of the mirrors are less than 10° to reduce the astigmatism due to folding. Lengths of the four arms of the resonator cavity are L₁ = 245 mm, L₂ = 355 mm, L₃ = 990 mm, and L₄ = 125 mm. Based on the ABCD matrix theory, spot radius of the oscillating light at S₁ on left end face of the Nd:YVO₄ crystal is calculated to be approximately 209 μm, which is consistent with the 200-μm spot radius of the pumping light.

IV. EXPERIMENTAL RESULTS

Before inserting the SA into the laser resonator, no mode-locking phenomenon is found although different positions of the SA in the cavity are adjusted, where the self-mode-locking behavior is excluded. With the perovskite nanoarrays as the SA, the optical spectrum of continuous wave and continuous wave mode locking (CWML) under the absorbed pump power of 5.4 W are illustrated in Fig. 6(a), with the 3-dB bandwidths of 0.12 nm and 0.16 nm at the central wavelength of 1064.63 nm and 1064.61 nm, respectively. With the perovskite nanoarrays as the SA, relationship between the output power and the absorbed pump power is shown in Fig. 6(b).

As can be clearly seen in Fig. 6(b), output power of continuous wave (CW) increases linearly from 2.96 mW to 1304 mW under the change of absorbed pump power from 1 W to 8 W, showing a conversion efficiency of 16.8% and a slope efficiency of 20.5%. Output power of the laser under mode-locking state is smaller than that under continuous-wave state, coming from the absorption property of perovskite. However, pillared perovskite has a higher conversion efficiency of 10.1% than thin films of 6.2%, which is consistent with the result mentioned above. In experiment, a fast photodiode (Newport Model 818-BB-21) is used to receive the mode-locked laser output from the 1064-nm all-solid-state passive mode-locked laser, and a digital oscilloscope (Agilent MSO7052B) is used to measure pulse waveform of the mode-locked laser. When the absorbed pump power is low, intensity of the laser in resonator do not reach the saturation threshold of perovskite, and the laser is operated in the Q-switched mode-locked state. With the continued increase of the absorbed pump power, intensity of the laser in the resonant cavity increases simultaneously. Continuous wave mode locking

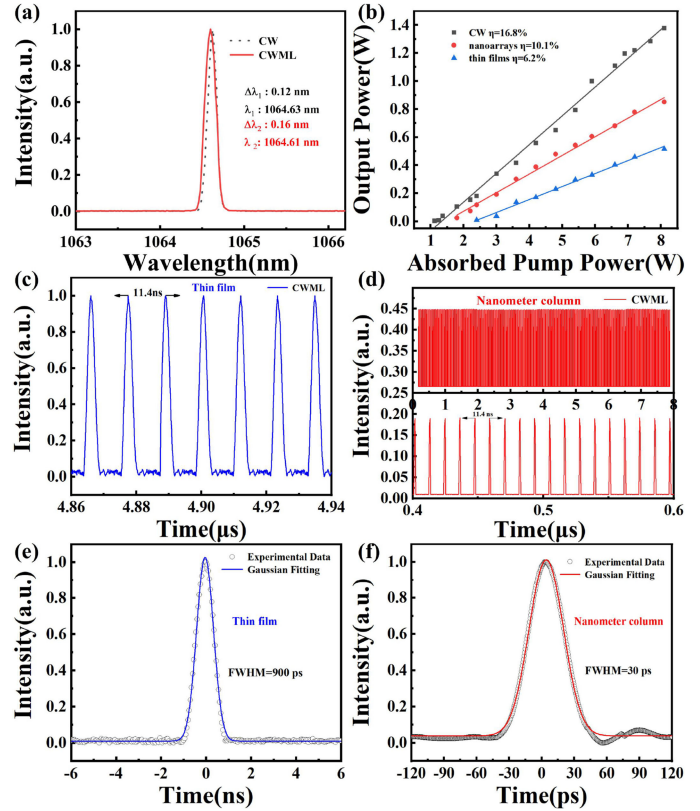


Fig. 6. Performance of the mode locked laser with the perovskite nanoarray as absorber. (a) Optical spectrum of laser; (b) Output power of the laser as a function of the absorbed pump power; (c) CWML pulse waveform of the laser at absorbed pump power of 5.4 W of the thin perovskite film; (d) CWML pulse waveform of perovskite nanoarrays at 5.4 W absorbed pump power; (e) (f) Autocorrelation curve of the pulse of the mode-locked laser.

(CWML) begins when the absorbed pump power exceeds 2.7 W and 3.2 W, with a SA of perovskite nanoarrays and perovskite thin films respectively. The mode-locked laser pulse with maximum output power of 542 mW and 334 mW are obtained, when the absorbed pump power reaches 5.4 W and 6 W, corresponding to perovskite nano-array and perovskite thin film respectively. The CWML pulses of the perovskite nanoarrays and perovskite thin films under an absorption pump power of 5.4 W are shown in Fig. 6(c) and (d), respectively. Pulse intervals are evenly distributed, and the amplitude is relatively stable. Interval of the pulses is approximately 11.4 ns, which corresponds to a repetition frequency of 87.3 MHz, determined by length of the cavity. An auto correlator is used to receive the mode-locked pulse output from the laser. The pulse width measured under an absorbed pump power of 5.4 W is shown in Fig. 6(e) and (f). The half-width full height of the measured pulses based on perovskite thin films and perovskite nanoarrays are approximately 900 ps and 30 ps, respectively. The time bandwidth product pulse based on perovskite nanoarrays is calculated to be approximately 1.2, which is larger than the transform-limited value of 0.441 for Gaussian pulses, which indicates that the CWML pulses are frequency chirped, and the pulse width could be further narrowed.

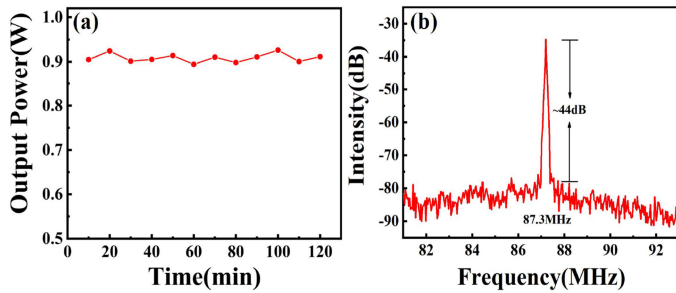


Fig. 7. The output characteristic of laser. (a) The output power of a continuous laser varies with time. (b) The RF spectrum of the CWML laser.

TABLE I
SUMMARY OF LASER WITH SAS BASED ON PEROVSKITE

Sample	Structure type	Modulation depth	Saturable intensity	Running condition	Wavelength	Pulse width	Ref
CsPbBr ₃	thin film	13.1%	10.7 MW/cm ²	Mode-locked	1076 nm	216 ps	22
MAPbI ₃	thin film	4.29% (1030nm)	1.6 GW/cm ² (1030nm)	Mode-locked	1064 nm	931ps	24
MAPbI ₃	thin film	3.9%	6.5 MW/cm ²	Q-switched	1064 nm	192ns	28
MAPbI ₃	thin film	6.9%	7.97 MW/cm ²	Mode-locked	1064 nm	900ps	This work
MAPbI ₃	nanoarrays	8.1%	9.53 MW/cm ²	Mode-locked	1064 nm	30ps	This work

In order to verify the stability of mode-locked laser, we have measured the output power of the laser under the absorbed pump power of 5.4 W within 120 minutes. The output power of the laser fluctuated in a small range around 0.9 W, and the fluctuation range of the output power is less than 3%, indicating that the laser has good stability. The radio frequency (RF) spectrum indicates the stability of a single pulse at a certain repetition frequency. To further study the pulse stability, the radio frequency (RF) spectrum was recorded under the RBW of 100 Hz. Fig. 7 shows the RF spectrum of the mode-locked pulse under a repetition frequency of 87.3 MHz and an absorbed pump power of 5.4 W. The signal-to-noise ratio of the pulse is approximately 44 dB, which indicates that the mode-locked pulse is relatively stable.

Table I summarizes the properties of the lasers with perovskite thin films as SAs. The comparison in Table I shows that the perovskite nanoarrays have better properties and can obtain shorter pulses, and this result is consistent with the simulation results and comparison of pulse output characteristics. The unsaturated loss increases with the modulation depth, resulting in Q-switched mode-locked. Therefore, in order to get stable mode-locked pulses, it is necessary to select the appropriate modulation depth, not the greater the better.

V. CONCLUSION

In summary, nanostructure CH₃NH₃PbI₃ nanorods have been proved to achieve low light loss and shorter pulses. The prepared perovskite is characterized by scanning electron microscopy, spectrophotometry and equilibrium synchronous dual detection technology. Optical properties of the saturated perovskite absorber such as the absorption spectrum, modulation depth and saturation intensity, are determined. The perovskite precursor

solution is confined in the pore by using an ultrathin AAO film, and the perovskite nanoarray is finally grown. A stable 1064-nm mode-locked pulse is achieved, with a 30-ps pulse width and 87.3-MHz repetition rate measured by applying the CH₃NH₃PbI₃ nanoarray as the SA. Maximum output power of the laser is 542 mW under an absorbed pump power of 5.4 W.

REFERENCES

- [1] F. Bonaccorso, Z. Sun, T. Hasan, and A. C. Ferrari, "Graphene photonics and optoelectronics," *Nature Photon.*, vol. 4, no. 9, pp. 611–622, 2010.
- [2] J. Wang *et al.*, "Evanescent-light deposition of graphene onto tapered fibers for passive Q-switch and mode-locker," *IEEE Photon. J.*, vol. 4, no. 5, pp. 1295–1305, Oct. 2012.
- [3] L. Wang *et al.*, "Sub-50 fs pulse generation from a SESAM mode-locked tm, Ho-codoped calcium aluminate laser," *Opt. Lett.*, vol. 46, no. 11, pp. 2642–2645, 2021.
- [4] J. Y. Huang, S. C. Huang, H. L. Chang, K. W. Su, Y. F. Chen, and K. F. Huang, "Passive Q switching of Er-Yb fiber laser with semiconductor saturable absorber," *Opt. Exp.*, vol. 16, no. 5, pp. 3002–3007, 2008.
- [5] J. Heidrich, M. Gaulke, B. O. Alaydin, M. Golling, A. Barh, and U. Keller, "Full optical SESAM characterization methods in the 1.9 to 3- μ m wavelength regime," *Opt. Exp.*, vol. 29, no. 5, pp. 6647–6656, 2021.
- [6] L. S. Liu *et al.*, "Wavelength-changeable thulium-doped fiber laser based on monolayer graphene," *Opt. Laser Technol.*, vol. 139, 2021, Art. no. 106980.
- [7] S. F. Zhang *et al.*, "Photonic-crystal-based broadband graphene saturable absorber," *Opt. Lett.*, vol. 44, no. 19, pp. 4785–4788, 2019.
- [8] R. I. Woodward *et al.*, "Wideband saturable absorption in few-layer molybdenum diselenide (MoSe₂) for Q-switching Yb-, Er- and Tm-doped fiber lasers," *Opt. Exp.*, vol. 23, no. 15, pp. 20051–20061, 2015.
- [9] W. J. Liu *et al.*, "Nonlinear optical properties of MoS₂-WS₂ heterostructure in fiber lasers," *Opt. Exp.*, vol. 27, no. 5, pp. 6689–6699, 2019.
- [10] C. X. Zhang *et al.*, "Sub-hundred nanosecond pulse generation from a black phosphorus Q-switched Er-doped fiber laser," *Opt. Exp.*, vol. 28, no. 4, pp. 4708–4716, 2020.
- [11] K. Wu *et al.*, "Recent progress of pulsed fiber lasers based on transition-metal dichalcogenides and black phosphorus saturable absorbers," *Nanophotonics*, vol. 9, no. 8, pp. 2215–2231, 2020.
- [12] L. Maserati *et al.*, "Photo-electrical properties of 2D quantum confined metal-organic chalcogenide nanocrystal films," *Nanoscale*, vol. 13, no. 1, pp. 233–241, 2021.
- [13] A. K. Jena, A. Kulkarni, and T. Miyasaka, "Halide perovskite photo-voltaics: Background, status, and future prospects," *Chem. Rev.*, vol. 119, no. 5, pp. 3036–3103, 2019.
- [14] J. Shamsi, A. S. Urban, M. Imran, and L. Manna, "Metal halide perovskite nanocrystals: Synthesis, post-synthesis modifications and their optical properties," *Chem. Rev.*, vol. 119, no. 5, pp. 3296–3348, 2020.
- [15] A. Jain, O. Voznyy, and X. Z. Lan, "Efficient and stable solution-processed planar perovskite solar cells via contact passivation," *Science*, vol. 355, no. 6362, pp. 722–726, 2017.
- [16] G. C. Xing *et al.*, "Low-temperature solution-processed wavelength-tunable perovskites for lasing," *Nature Mater.*, vol. 13, no. 5, pp. 476–480, 2014.
- [17] W. S. Yang *et al.*, "Iodide management in formamidinium-lead-halide-based perovskite layers for efficient solar cells," *Science*, vol. 356, no. 6345, pp. 1376–1379, 2017.
- [18] L. N. Quan, B. P. Rand, R. H. Friend, S. G. Mhaisalkar, T. W. Lee, and E. H. Sargent, "Perovskites for next-generation optical sources," *Chem. Rev.*, vol. 119, no. 12, pp. 7444–7477, 2019.
- [19] S. Yakunin *et al.*, "Low-threshold amplified spontaneous emission and lasing from colloidal nanocrystals of caesium lead halide perovskites," *Nat. Commun.*, vol. 6, 2015, Art. no. 8515.
- [20] H. T. Wei *et al.*, "Sensitive X-ray detectors made of methylammonium lead tribromide perovskite single crystals," *Nat. Photon.*, vol. 10, no. 5, pp. 333–339, 2016.
- [21] J. S. Manser, J. A. Christians, and P. V. Kamat, "Intriguing optoelectronic properties of metal halide perovskites," *Chem. Rev.*, vol. 116, no. 21, pp. 12956–13008, 2016.

- [22] Y. Zhou, Z. P. Hu, Y. Li, J. Q. Xu, X. S. Tang, and Y. L. Tang, "CsPbBr₃ nanocrystal saturable absorber for mode-locking ytterbium fiber laser," *Appl. Phys. Lett.*, vol. 108, no. 26, 2016, Art. no. 261108.
- [23] R. Zhang *et al.*, "Nonlinear optical response of organic-inorganic halide perovskites," *ACS Photon.*, vol. 3, no. 3, pp. 371–377, 2016.
- [24] P. F. Li *et al.*, "Two-Dimensional CH₃NH₃PbI₃ perovskite nanosheets for ultrafast pulsed fiber lasers," *ACS Appl. Mater. Interfaces*, vol. 9, no. 14, pp. 12759–12765, 2017.
- [25] G. B. Jiang *et al.*, "Ultrafast pulse generation from erbium-doped fiber laser modulated by hybrid organic-inorganic halide perovskites," *Appl. Phys. Lett.*, vol. 110, no. 16, 2017, Art. no. 161111.
- [26] J. Yi, L. L. Miao, J. Li, W. Hu, C. J. Zhao, and S. C. Wen, "Third-order nonlinear optical response of CH₃NH₃PbI₃ perovskite in the mid-infrared regime," *Opt. Mater. Exp.*, vol. 7, no. 11, pp. 3894–3901, 2017.
- [27] L. Miao *et al.*, "Erbium-doped fiber laser mode-locked by halide perovskite via evanescent field interaction," *IEEE Photon. Technol. Lett.*, vol. 30, no. 6, pp. 577–580, Mar. 2018.
- [28] J. Wang, Y. G. Wang, Z. D. Chen, X. G. Yang, and R. D. Lv, "CH₃NH₃PbI₃ perovskite thin films as a saturable absorber for a passively Q-switched Nd:YAG laser," *J. Mater. Chem. C*, vol. 7, no. 17, pp. 5047–5050, 2019.
- [29] J. Wang *et al.*, "1.34 μm Q-switched Nd:YVO₄ laser based on perovskite film saturable absorber," *IEEE Photon. Technol. Lett.*, vol. 32, no. 1, pp. 3–6, Jan. 2020.
- [30] K. Seeger. *Semiconductor Physics[M]*. Berlin, Germany: Springer-Verlag, 1985.